Available online at www.sciencedirect.com

ScienceDirect

Energy Procedia 102 (2016) 43 – 48

Energy Procedia

E-MRS Spring Meeting 2016 Symposium T - Advanced materials and characterization techniques for solar cells III, 2-6 May 2016, Lille, France

Back- and front-side texturing for light-management in perovskite / silicon-heterojunction tandem solar cells

M. Jošt[a,c]*, S. Albrecht[b], B. Lipovšek[a], J. Krč[a], L. Korte[b], B. Rech[b,c] and M. Topič[a]

[a]*University of Ljubljana, Faculty of Electrical Engineering, Tržaška cesta 25, 1000 Ljubljana, Slovenia*
[b]*Helmholtz-Zentrum Berlin für Materialien und Energie GmbH, Institut für Silizium-Photovoltaik, Kekuléstraße 5, 12489 Berlin, Germany*
[c]*Technische Universitaet Berlin, Fakultät IV - Elektrotechnik und Informatik, Marchstraße 23, 10587 Berlin, Germany*

Abstract

The perovskite / silicon-heterojunction (SHJ) tandem solar cell can theoretically overcome the efficiencies of the single junction solar cells with experimental results not far behind. Here, we use optical simulations to analyze the potential of such currently feasible monolithic perovskite / SHJ tandem devices. We consider three different device designs in the optical simulations: planar device, device built on back-side textured Si wafer, and device with textured UV Nanoimprint Lithography light management foil. For each of these three designs, the current matching point is simulated to evaluate device efficiencies. While the device with back-side textured Si wafer causes light trapping and therefore enhanced photocurrent generation for longer wavelengths, the anti-reflection foils prove to be overall more efficient as the foil significantly reduces the reflection in almost full wavelength range.

Keywords: perovskite solar cells; silicon-heterojunction; monolithic tandem solar cell; optical simulation; textured interfaces; UV NIL layer; device optimization.

1. Introduction

The perovskite / silicon-heterojunction (SHJ) tandem solar cell is an interesting candidate to exceed the Shockley-Queisser limit [1]–[3] for single junction solar cells due to the high conversion efficiency of both solar cells [4], [5]

* Corresponding author. Tel.: +386 1 4768 723; fax: +386 1 4264 630.
E-mail address: marko.jost@fe.uni-lj.si

doi:10.1016/j.egypro.2016.11.316

and their complementary band-gaps. By tuning the band-gap of the perovskite [6] we can even reach the optimum ratio of 1.73 eV to 1.12 eV [7], [8]. The optical simulations have indeed shown the potential in both monolithic and 4-terminal configuration [7], [9] followed by the experimental attempts that also show promising results [10]–[12]. Compared to 4- terminal devices which have two separate solar cells stacked one above the other, monolithic devices have 2 subcells connected in series and processed sequentially. Series connection results in a higher voltage of the full device since the voltages of the two subcells are summed. However, to reach the optimum efficiency, the current of the subcells has to match.

Currently, most of the experimental monolithic tandem devices have planar configuration and are therefore partially limited by photocurrent generation. Further gains in photocurrents can be achieved by introducing structures for light scattering and anti-reflection (AR) [11]. However, commonly used random pyramid texturization of silicon wafers is not yet suitable for the deposition of thin perovskite layers when implementing deposition techniques such as spin coating that gives the highest efficiencies to date. An alternative way to reduce optical losses on planar wafers is utilizing UV Nanoimprint Lithography (UV NIL). UV NIL is a replication process where texture from the master can be transferred on the substrate using mechanical deformation of the UV sensitive polymers [13]–[16]. Therefore, with UV NIL an additional transparent textured layer on top of the planar tandem (or single junction) cell can be created that enables light scattering or/and AR.

In our contribution, we focus on the optical optimization of planar monolithic perovskite / SHJ tandem solar cell by means of optical simulations for the currently feasible fabrication processes. First, random pyramids of the silicon wafer on the back side only are considered. Second, light management with randomly distributed pyramids deposited on the top of the planar tandem cell (ITO) by UV NIL process is investigated. For the selected device architectures, we optimize the thickness of the perovskite layer to achieve current matching in monolithic perovskite / SHJ tandem solar cell. This current is then used, together with experimentally achievable performance parameters, to estimate the efficiencies of the investigated device designs. The results show that using the textured surfaces we can improve the performance compared to the planar device.

2. Optical model description

For the purpose of this study we base our optical simulations on the monolithic planar perovskite/ SHJ tandem solar cell shown in Fig. 1a and presented in [12]. In the proposed configuration, the top cell is a perovskite solar cell with the band-gap of 1.54 eV as found in the literature [17] and in agreement with the quantum efficiency measurement. Despite being 0.19 eV away from the optimum band-gap, this should still result in high efficiencies and the effect of different textures can be translated to the case with a slightly higher perovskite band-gap. Since the SHJ solar cell is already well optimized, we keep its structure as a constant and only focus on the perovskite absorbing layer to achieve the highest possible current matching point.

The optical simulator CROWM [18], which is based on a combined ray and wave optics model, was used to conduct optical simulations. The n and k files needed to conduct the simulations were obtained using the reflectance/transmittance (RT) method, found in the internal library or from the literature for spiro-OMeTAD and perovskite [9], [17]. The outputs of the simulator are total reflection, transmission, and absorption in each layer, which integrated equals to the short-circuit current density J_{SC} or equivalent current density loss in the individual layer. The simulations were carried out in the wavelength range from 350 to 1200 nm.

We considered three main cases in our simulations as shown in Fig. 1. Fig. 1a shows the planar device as was proposed and fabricated by Albrecht et al. [12]. Derived from this structure, there are two main currently feasible possibilities of implementing textured surfaces to cause light management. Option 1 is to start with a one-side textured silicon wafer and deposit the layers on the textured surface towards the bottom conformally, while depositing the layers to the top as in the planar device (Fig. 1b). Option 2 is currently much more attractive and is shown in Fig. 1c. Here, we keep the planar structure and add either a textured anti-reflection foil or, as will be discussed in this paper, a textured UV NIL layer on top of the device. UV NIL process allows us to use a texture of our choice (as long as a master with the same texture can be provided). For our analysis of the UV NIL light management layer (see Fig. 2a

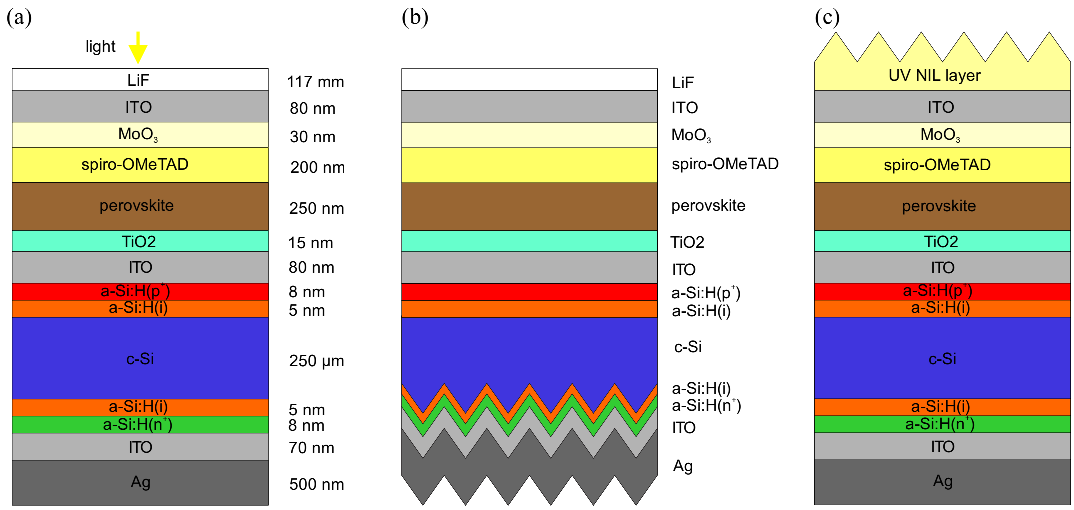

Fig. 1: Schematic illustration of the investigated perovskite / SHJ tandem devices (a) planar, (b) back-sided textured Si wafer and (c) planar design with textured UV NIL layer.

for SEM of UV NIL replica), we chose randomly distributed pyramids from a Si wafer that are known for their excellent anti-reflection properties. In this case, UV NIL layer replaced the LiF anti-reflective coating used in the other two cases. The refractive index of the LiF is 1.39 and therefore almost ideal for the air/ITO interface, while the refractive index of the UV NIL lacquer is 1.54.

As the analysis of the devices with the textured surfaces requires much computational time, we decided to keep the thicknesses as shown in Fig. 1a and only alter the perovskite absorber thickness in order to reach the current matching point. Compared to the report by Filipic et al. [9] we performed the simulations for the back-side texture and the textured UV NIL light management foil, and compared to Albrecht et al. [7] we considered textured interfaces in our structure, albeit not for the optimum perovskite band-gap.

3. Results

The results of the optical simulations for the three cases depicted in Fig. 1 are presented in Table 1. Both the back-side textured Si wafer and the UV NIL layer have randomly distributed pyramids as a texture. Using the textures, we can indeed reduce the reflection, namely for 2.5 mA cm^{-2} with the back-side textured Si wafer and almost 4 mA cm^{-2} with the proposed UV NIL layer. The so-gained light is then absorbed in the absorbing layers with the extracted current increased from 16.23 mA cm^{-2} for the planar device to 16.94 mA cm^{-2} and 17.51 mA cm^{-2} for the back-side textured Si wafer and the UV NIL layer device, respectively. Since the SHJ bottom cell is kept as a constant and the amount of light absorbed within is increased, the perovskite absorber must be thicker to absorb more light for the current matching point to be reached (see Table 1). Interestingly, for the same thickness of the perovskite layer we get much more current with the UV NIL layer as compared to the back-side textured Si wafer. We attribute this to less reflection losses, which are lower for the wavelengths below 1050 nm for the device with the UV NIL layer. We can also estimate the efficiency we could reach by assuming the experimentally achievable parameters [12] open circuit voltage (V_{OC}) to be 1.80 V (1.10 V for perovskite and 0.70 V for SHJ solar cell) and a fill factor (FF) of 0.80. For the cases presented here the highest efficiency would be 25.21%. This means a 7.9% increase over the planar device performance.

Table 1: Short circuit current (J_{SC}) and equivalent reflection loss in a current matching point for the three device designs from Fig. 1 and estimated efficiency based of experimentally achievable parameters of the open circuit voltage (V_{OC}) and fill factor (FF). Perovskite layer thickness in the current matching point is also stated.

	R_{tot} (mA cm^{-2})	PK thickness	J_{SC} (mA cm^{-2})	V_{OC} (V)	FF	Eff (%)	Change
Planar	9.53	250 nm	16.23			23.37	0
Back-textured	7.02	280 nm	16.94	1.80	0.80	24.39	4.4%
UV NIL	5.67	280 nm	17.51			25.21	7.9%

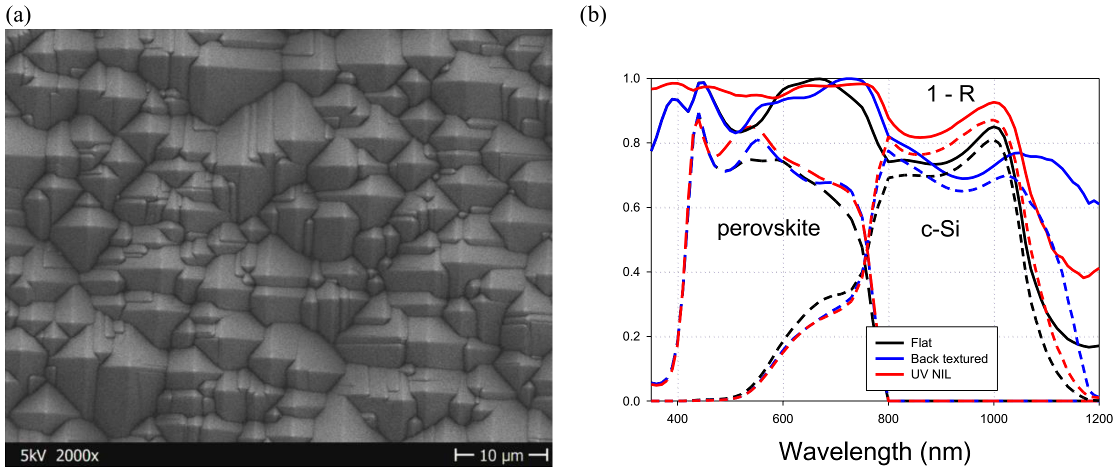

Fig. 2: (a) SEM image of randomly distributed pyramids from the UV NIL replica of the textured Si wafer and (b) Reflection and absorption spectra for all three device designs (flat device, back-side textured Si wafer and UV NIL light management foil).

Fig. 2b shows the reflection (1-R) and the absorption for the three studied cases. The reflection with the back-side texture is mostly reduced for the long-wavelength region, where we also get the highest increase in the current in the c-Si due to light trapping. However, it has little effect on the device performance in the visible light region as only wavelengths above 1000 nm can reach the back side of the device. Therefore, one would expect that for the wavelengths below 1000 nm the absorption / reflection spectra would be the same for the back-side textured Si wafer and the planar device. This would be true if both devices had the same perovskite absorber thickness. However, to reach the current matching point, we had to increase the thickness of the perovskite absorber layer, which resulted in different interferences and therefore different absorption spectra. Compared to the back-side textured Si wafer, the UV NIL layer is more effective as an anti-reflection layer as the reflection is decreased in the whole wavelength range. Consequently, compared to the planar device, the absorption is also increased for all wavelengths. Still, for longer wavelengths the texture on the back side is more effective than that on the front side. Thus, we would get best results with the two textures combined.

4. Conclusions

We presented the optical simulations of perovskite / SHJ tandem solar cells with three different device designs. We introduced a back-side textured Si wafer solar cell to induce light scattering and a textured UV NIL layer on the front side in order to optimize light management. The back-side textured Si surface only increased the current density by 0.7 mA cm^{-2} compared to the planar device structure. This increase is caused by the prolonged optical path in the near infrared (NIR) region and results in the 24.4-% efficiency of this device design if we assume V_{OC} =1.80 V and FF =

0.80. The textured UV NIL layer performs better; the current increase amounts to 1.3 mA cm^{-2} due to the reduced reflection, resulting in a 25.2-% efficiency. Textured surfaces in both device designs increase the current in c-Si. Therefore, to reach the current matching point we also have to increase the perovskite absorber layer thickness, in our case for 30 nm.

The device architectures were only optimized for the perovskite absorber layer thickness at a fixed perovskite bandgap of 1.54 eV. Nevertheless, we show that the improvement using textures is significant. However, there is still room for optimization. Further improvements can be achieved by using perovskite with the optimal bandgap, optimizing the thicknesses of all layers and combining front- and back-side texture. This way, we anticipate the conversion efficiency to exceed 30%.

Acknowledgement

The authors are grateful to Carola Klimm, Institute for Silicon Photovoltaics, HZB for performing SEM measurements. The authors acknowledge the financial support from the Slovenian Research Agency (program P2-0197 and project J2-5466). M.J. thanks the Slovenian Research Agency for his PhD funding and Slovene Human Resources Development and Scholarship Fund for his research stay scholarship.

References

[1] W. Shockley and H. J. Queisser, "Detailed Balance Limit of Efficiency of p-n Junction Solar Cells," *J. Appl. Phys.*, vol. 32, no. 3, pp. 510–519, Mar. 1961.
[2] M. Jošt and M. Topič, "Efficiency limits in photovoltaics: Case of single junction solar cells," *Facta Univ. - Ser. Electron. Energ.*, vol. 27, no. 4, pp. 631–638, 2014.
[3] A. D. Vos, "Detailed balance limit of the efficiency of tandem solar cells," *J. Phys. Appl. Phys.*, vol. 13, no. 5, p. 839, 1980.
[4] M. Saliba, T. Matsui, J.-Y. Seo, K. Domanski, J.-P. Correa-Baena, M. K. Nazeeruddin, S. M. Zakeeruddin, W. Tress, A. Abate, A. Hagfeldt, and M. Grätzel, "Cesium-containing triple cation perovskite solar cells: improved stability, reproducibility and high efficiency," *Energy Environ. Sci.*, Mar. 2016.
[5] K. Masuko, M. Shigematsu, T. Hashiguchi, D. Fujishima, M. Kai, N. Yoshimura, T. Yamaguchi, Y. Ichihashi, T. Mishima, N. Matsubara, T. Yamanishi, T. Takahama, M. Taguchi, E. Maruyama, and S. Okamoto, "Achievement of More Than 25 #x0025; Conversion Efficiency With Crystalline Silicon Heterojunction Solar Cell," *IEEE J. Photovolt.*, vol. 4, no. 6, pp. 1433–1435, Nov. 2014.
[6] S. A. Kulkarni, T. Baikie, P. P. Boix, N. Yantara, N. Mathews, and S. Mhaisalkar, "Band-gap tuning of lead halide perovskites using a sequential deposition process," *J. Mater. Chem. A*, vol. 2, no. 24, pp. 9221–9225, May 2014.
[7] S. Albrecht, M. Saliba, J.-P. Correa-Baena, K. Jäger, L. Korte, A. Hagfeldt, Michael Grätzel, and B. Rech, "Towards optical optimization of planar monolithic perovskite/silicon-heterojunction tandem solar cells," *J. Opt.*, vol. 18, no. 6, p. 064012, 2016.
[8] D. P. McMeekin, G. Sadoughi, W. Rehman, G. E. Eperon, M. Saliba, M. T. Hörantner, A. Haghighirad, N. Sakai, L. Korte, B. Rech, M. B. Johnston, L. M. Herz, and H. J. Snaith, "A mixed-cation lead mixed-halide perovskite absorber for tandem solar cells," *Science*, vol. 351, no. 6269, pp. 151–155, Jan. 2016.
[9] M. Filipič, P. Löper, B. Niesen, S. De Wolf, J. Krč, C. Ballif, and M. Topič, "CH_3NH_3PbI_3 perovskite / silicon tandem solar cells: characterization based optical simulations," *Opt. Express*, vol. 23, no. 7, p. A263, Apr. 2015.
[10] P. Löper, S.-J. Moon, S. M. de Nicolas, B. Niesen, M. Ledinsky, S. Nicolay, J. Bailat, J.-H. Yum, S. D. Wolf, and C. Ballif, "Organic–inorganic halide perovskite/crystalline silicon four-terminal tandem solar cells," *Phys. Chem. Chem. Phys.*, vol. 17, no. 3, pp. 1619–1629, Dec. 2014.

[11] J. Werner, C.-H. Weng, A. Walter, L. Fesquet, J. P. Seif, S. De Wolf, B. Niesen, and C. Ballif, "Efficient Monolithic Perovskite/Silicon Tandem Solar Cell with Cell Area >1 cm2," *J. Phys. Chem. Lett.*, pp. 161–166, Dec. 2015.

[12] S. Albrecht, M. Saliba, J. P. C. Baena, F. Lang, L. Kegelmann, M. Mews, L. Steier, A. Abate, J. Rappich, L. Korte, R. Schlatmann, M. K. Nazeeruddin, A. Hagfeldt, M. Grätzel, and B. Rech, "Monolithic perovskite/silicon-heterojunction tandem solar cells processed at low temperature," *Energy Environ. Sci.*, vol. 9, no. 1, pp. 81–88, Jan. 2016.

[13] S. Y. Chou, P. R. Krauss, and P. J. Renstrom, "Nanoimprint lithography," *J. Vac. Sci. Technol. B*, vol. 14, no. 6, pp. 4129–4133, Nov. 1996.

[14] J. Escarré, C. Battaglia, K. Söderström, C. Pahud, R. Biron, O. Cubero, F.-J. Haug, and C. Ballif, "UV imprinting for thin film solar cell application," *J. Opt.*, vol. 14, no. 2, p. 024009, Feb. 2012.

[15] M. Meier, U. W. Paetzold, M. Ghosh, and A. J. M. van Erven, "Nano-imprint lithography for advanced light management concepts in multi-junction solar cells," in *Photovoltaic Specialist Conference (PVSC), 2014 IEEE 40th*, 2014, pp. 2836–2838.

[16] M. Jošt, M. Berginc, Čampa, J. Krč, P. Panjan, B. Malič, and M. Topič, "Nanoimprinted textures on glass as a substrate for GITO deposition," presented at the 51th International Conference on Microelectronics, Devices and Materials and the Workshop on Terahertz and Microwave Systems, Bled, Slovenija, 2015, vol. 2015, pp. 23–28.

[17] P. Löper, M. Stuckelberger, B. Niesen, J. Werner, M. Filipič, S.-J. Moon, J.-H. Yum, M. Topič, S. De Wolf, and C. Ballif, "Complex Refractive Index Spectra of CH3NH3PbI3 Perovskite Thin Films Determined by Spectroscopic Ellipsometry and Spectrophotometry," *J. Phys. Chem. Lett.*, vol. 6, no. 1, pp. 66–71, Jan. 2015.

[18] B. Lipovsek, J. Krč, and M. Topič, "Optical model for thin-film photovoltaic devices with large surface textures at the front side," *Inf. MIDEM*, vol. 41, no. 4, pp. 264–271, Dec. 2011.